

# Effect of fluid rheology on particle migration in a square-shaped microchannel

Francesco Del Giudice · Gaetano D'Avino ·  
Francesco Greco · Paolo A. Netti · Pier Luca Maffettone

Received: 14 May 2014 / Accepted: 25 January 2015 / Published online: 19 February 2015  
© Springer-Verlag Berlin Heidelberg 2015

**Abstract** The effect of fluid rheology on particle migration induced by fluid viscoelasticity in a square-shaped microchannel is reported. Three water polymer solutions of PolyEthylene Oxyde at different concentrations, corresponding to different elasticity and degree of shear thinning, are prepared and rheologically characterized. Experiments are carried out for a wide range of flow rates, and the particle distributions over the channel cross section are reconstructed by combining particle tracking measurements and numerical simulations of the fluid velocity profile. The particle distributions show that the migration direction strongly depends on the fluid rheology. Specifically, when particles explore the constant viscosity region of the suspending liquids, they are focused around the channel centerline. Such an effect is more and more pronounced as the flow rate increases. On the other hand, for particles suspended in a shear-thinning fluid, a different scenario appears: At low flow rates, i.e., in the constant viscosity region, particles still migrate toward the channel centerline, while at high flow rates, i.e., in the shear thinning region, the migration reverts direction and the particles are driven toward the corners of the channel cross section. Those

experimental observations elucidate the relevant and competing role of elasticity and shear thinning, with obvious implications in designing microfluidic devices for particle manipulation. Finally, our results highlight the weak effect of inertia on particle migration as compared to viscoelastic effects, even for low elastic suspending liquids.

**Keywords** Microfluidic · Migration · Viscoelasticity · Shear thinning · Rheology

## 1 Introduction

In recent years, suspensions of particles flowing in microfluidic channels have received great interest. Indeed, the possibility of manipulating the particle trajectories in microchannels opens up the way to several microfluidic operations useful in biology and chemistry, e.g., cytometry, separation, detection and analysis (Whitesides 2006; Pamme 2007; Bhagat et al. 2010; Nam et al. 2012; Yang et al. 2012).

It is well known that particles suspended in Newtonian fluids flowing in a channel at low Reynolds numbers passively follow the flow field streamlines (Ho and Leal 1974). On the other hand, a force transversal to the flow direction is required in order to drive particles toward specific channel regions. Along with external forces generated, for instance, by electric (Xuan et al. 2010; Liang et al. 2010; Zande et al. 1999; Cavallaro et al. 2011), magnetic (Gijs 2004; Pamme 2006; Yamaguchi et al. 1990; Zeng et al. 2013) or acoustic fields (Yeo and Friend 2014; Shields et al. 2014; Skowronek et al. 2013), a cross-streamline particle migration can also be promoted by 'inner' forces, i.e., forces that are directly generated by the flow of the suspending fluid (Leshansky et al. 2007; Di Carlo 2009; Lee et al. 2013).

---

F. Del Giudice (✉) · P. A. Netti · P. L. Maffettone  
Center for Advanced Biomaterials for Health Care @CRIB,  
Istituto Italiano di Tecnologia, P.le Tecchio 80, 80125 Naples,  
Italy  
e-mail: francesco.delgiudice@me.com

F. Del Giudice · G. D'Avino · P. A. Netti · P. L. Maffettone  
Dipartimento di Ingegneria Chimica, dei Materiali e della  
Produzione Industriale, Università di Napoli Federico II,  
P.le Tecchio 80, 80125 Naples, Italy

F. Greco  
Istituto di Ricerche sulla Combustione, IRC-CNR,  
P.le Tecchio 80, 80125 Naples, Italy

For Newtonian liquids at high flow rate, the Reynolds number may become relevant even in microfluidic devices, and inertia starts to play a role. In those conditions, inertial forces arise, pushing the suspended particles toward specific equilibrium positions within the channel cross section, depending on channel geometry (Di Carlo 2009; Choi et al. 2011; Zhou and Papautsky 2013). In cylindrical channels, the particles are driven toward an equilibrium radial position between the channel centerline and the wall, a spectacular manifestation of the inertia effects known as the Segré-Silberberg effect (Segré and Silberberg 1961). In channels with a square-shaped cross section, the particles migrate toward four equilibrium positions located near the center of the channel side (Di Carlo 2009; Choi et al. 2011). It is clear that particle alignment, i.e., migration of particles along a unique streamline, is not possible by exploiting inertial effects in straight channels. Indeed, more complex channel designs have been proposed in the last decades allowing to use inertial forces to drive all of microparticles to a streamline (Zhou and Papautsky 2013; Martel and Toner 2013).

Recently, an alternative way to induce a transversal force on particles in a microchannel, based on viscoelasticity of the flowing suspending fluid, has been demonstrated both theoretically and experimentally (Leshansky et al. 2007; Yang et al. 2011; D'Avino et al. 2012; Del Giudice et al. 2013). Indeed, the elastic nature of the suspending liquid gives rise to an imbalance of normal stresses around the particle surface, producing a net migration force transversally to the flow direction (Leshansky et al. 2007; Romeo et al. 2013). The migration direction has been found to depend on the shape of the channel cross section (Leshansky et al. 2007; Yang et al. 2011; D'Avino et al. 2012; Del Giudice et al. 2013), the particle-to-channel size ratio (D'Avino et al. 2012; Lim and Nam 2014) and the fluid rheology (Villone et al. 2013; Lim and Nam 2014; Kang et al. 2013). Experiments in cylindrical (D'Avino et al. 2012; Romeo et al. 2013) or wide-slit (Leshansky et al. 2007) microchannels evidenced that an elastic constant viscosity fluid (aqueous solution of polyvinylpyrrolidone, PVP) promotes migration toward the centerline or centerplane, respectively. Shear thinning seems to invert the migration direction for those particles traveling near the walls (D'Avino et al. 2012), although only a single observation of such phenomenology is reported. A reduction of the focusing mechanism in shear-thinning fluids has also been very recently shown (Seo et al. 2014). More intriguing is the behavior in square-shaped microchannels. For the same PVP fluid, the particles are observed to move both toward the centerline and the corners (Yang et al. 2011). A similar scenario is found for a low concentrated

PolyEthylene Oxyde (PEO) solution at low flow rates (Yang et al. 2011). Increasing the flow rate, but below a critical value, all the flowing particles are focused on the centerline. This behavior has been attributed to the competition between inertial and viscoelastic effects (Yang et al. 2011). More recently, very same experiments in PVP report the focusing on the centerline at any flow rate investigated, in sharp contrast with previous observations (Yang et al. 2011). Finally, in microchannels with non-circular cross sections, recent works have been focused on the competition between migration and secondary flows (Villone et al. 2013; Lim and Nam 2014). Lim et al. (2014) showed experimentally that secondary flows, generated from the second normal stress difference, affect the focusing mechanism because a new equilibrium position appears, confirming numerical simulations (Villone et al. 2013). Villone et al. (2013) also reported that a particle suspended in a shear-thinning fluid migrates toward different equilibrium positions depending on the fluid elasticity and the degree of shear thinning.

It so appears that the available literature shows a number of different behaviors as the suspending fluid is varied, sometimes with conflicting results (Yang et al. 2011; Del Giudice et al. 2013), so that the link between rheology and migration is not clear yet. Needless to say, understanding the role of the fluid rheology helps to optimize existing devices and to possibly design novel microfluidic processes for particle manipulation.

In this work, we attempt to elucidate the influence of the suspending fluid rheological properties (elasticity and shear thinning) on the migration phenomenon. To this aim, three viscoelastic liquids, characterized by different elasticity and severity of viscous dissipation and shear thinning, have been prepared and rheologically characterized. Migration experiments in a square-shaped microchannel at different imposed flow rates have been performed. The particle positions in the channel cross section are reconstructed by combining particle tracking measurements and numerical simulations of the velocity profile of the unloaded fluids in the same geometrical and flow conditions [such a procedure for obtaining the particle positions within the cross section of the channel has been described in detail elsewhere (Del Giudice et al. 2013)]. The particle distributions through the channel section, directly obtained from the particle positions, are thus related to the fluid rheology, clarifying its role on the migration mechanism. Some further results on the competition between viscoelastic and inertial effects are also reported, discussing the relevance of the Elasticity number, extensively used in previous works (Yang et al. 2011; Nam et al. 2012; Del Giudice et al. 2013; Romeo et al. 2013; Lim and Nam 2014), to quantify the competition between inertia and viscoelasticity.

## 2 Dimensionless parameters

It is useful to define some dimensionless parameters to be used in the following sections. The entity of fluid viscoelasticity can be quantified by the Deborah number defined, for a square-shaped channel, as:

$$De = \frac{\lambda}{t_f} = \frac{\lambda Q}{H^3} \tag{1}$$

where  $\lambda$  is the fluid relaxation time,  $Q$  is the volumetric flow rate, and  $H$  is the side of the channel cross section. The Deborah number is the ratio between the fluid relaxation time  $\lambda$  and the flow characteristic time  $t_f = H^3/Q$ . When  $De = 0$ , the fluid is Newtonian (because  $\lambda = 0$ ), whereas increasing  $De$  corresponds to more pronounced viscoelastic effects.

Another important parameter for the system under investigation is the Reynolds number:

$$Re = \frac{\rho Q}{\eta H} \tag{2}$$

with  $\rho$  and  $\eta$  the suspending fluid density and viscosity, respectively; the Reynolds number represents the ratio between inertial and viscous forces.

The ratio between the Deborah and Reynolds numbers defines the Elasticity number:

$$El = \frac{De}{Re} = \frac{\lambda \eta}{\rho H^2} \tag{3}$$

Viscoelastic or inertial forces are dominant when  $El \gg 1$  or  $El \ll 1$ , respectively, whereas, for  $El \sim 1$ , the viscoelastic forces are comparable with the inertial ones. It is worthwhile to notice that the Elasticity number only depends on the fluid properties and the characteristic channel dimension. For a given fluid and channel geometry, the value of the Elasticity number is then independent of the applied flow rate  $Q$ .

In the present work, the Deborah number ranges from very low values up to  $De = 9.2$ , where strong nonlinear effects are present. Therefore, we expect a Newtonian-like behavior for the lowest flow rates, and strong changes in the particle distributions at higher flow rates due to viscoelasticity-induced migration.

## 3 Materials and methods

### 3.1 Suspending fluids and particles

PolyEthylene Oxyde (PEO) with average molecular weigh  $M_w = 4000$  kDa (Sigma-Aldrich) and at three mass concentrations of 0.1, 0.8, 1.6 wt% in water were used. Glycerol (25 wt%) was added to the solutions in order to prevent

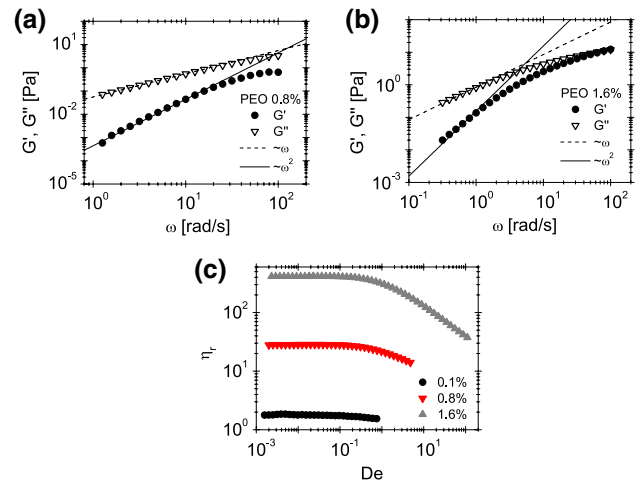


**Fig. 1** **a** Measured elastic modulus  $G'$  (black circles) and loss modulus  $G''$  (white triangles) for the aqueous PEO 0.8 wt%. **b** Measured elastic modulus  $G'$  (black circles) and loss modulus  $G''$  (white triangles) for the aqueous PEO 1.6 wt%. In both panels **a** and **b**, the slopes of the straight lines are 2 and 1 for  $G'$  and  $G''$ , respectively, and indicate the expected frequency dependence in the ‘terminal region’ of a viscoelastic fluid. **c** Measured steady relative shear viscosity  $\eta_r$  for the aqueous PEO solutions at different concentration as a function of the Deborah number  $De$ . The relative viscosity  $\eta_r$  is calculated with respect to the viscosity of the solvent (a glycerol–water mixture with  $\eta = 2 \times 10^{-3}$  Pa s)

particle sedimentation (Yang et al. 2011). The viscosity of the glycerol–water solution is  $\eta = 2 \times 10^{-3}$  Pa s.

The fluid rheological properties are measured by a stress-controlled rheometer (Anton Paar MCR 302 rheometer), with cone and plate geometry with diameters of 60 mm and with a solvent trap to avoid fluid evaporation. The fluids rheology is reported in Fig. 1.

Figure 1a, b reports the linear viscoelastic response for PEO 0.8 and 1.6 wt%, respectively, for an imposed deformation  $\gamma = 5\%$  and over two and three frequency decades, respectively. The PEO 0.8 % shows the typical trends of the moduli at low frequencies, i.e.,  $G' \propto \omega^2$  and  $G'' \propto \omega$ . Then, we estimate the fluid relaxation time by the intersection of the straight lines at low frequencies giving  $\lambda \sim 8 \times 10^{-3}$  s (D’Avino et al. 2012). By following the same procedure, we estimate the relaxation time of PEO 1.6 % as  $\lambda \sim 0.18$  s.

For the PEO at the lowest concentration, the moduli cannot be measured by our stress-controlled rheometer because of their very low values. Therefore, we decided to use the relaxation time predicted from the Zimm theory (Rodd et al. 2005, 2007) given by:

$$\lambda_{zimm} = \frac{f[\eta]M_w\eta_s}{RT} \tag{4}$$

where  $f$  is a prefactor dependent on the solvent quality,  $[\eta]$  is the intrinsic viscosity,  $M_w$  is the molecular weight,  $\eta_s$  is the solvent viscosity,  $R$  is the gas constant,

and  $T$  is the absolute temperature. For the fluid considered here, it is  $f = 0.463$  [for a good solvent (Rodd et al. 2005; Tirtaatmadja et al. 2006)] and  $\eta_s = 2 \times 10^{-3}$  Pa s,  $T = 295$  K. A measurement of the intrinsic viscosity of PEO 4 MDa in 25 wt% glycerol–water solution, available in the literature (Del Giudice et al. 2015), gives  $[\eta] = 0.8$  m<sup>3</sup>/kg. The resulting relaxation time from Eq. (4) is  $\lambda \sim 1.25 \times 10^{-3}$  s.

Notice that, strictly speaking, the Zimm prediction is valid in the dilute regime, i.e., when the concentration is lower than the so-called overlapping concentration  $c^*$ . An estimate of the latter through the intrinsic viscosity  $[\eta]$  can be obtained from the Flory theory (Tirtaatmadja et al. 2006) or from the Graessley expression (Graessley 1982). By using the above indicated value  $[\eta] = 0.8$  m<sup>3</sup>/kg, we obtain  $c^* = 1/[\eta] = 0.12$  g/dl (Flory) and  $c^* = 0.77/[\eta] = 0.096$  g/dl (Graessley). Both such estimates are close to the concentration  $c = 0.1$  g/dl under discussion here. Therefore, the use of the Zimm prediction for the relaxation time is deemed acceptable.

In addition, such estimate is in rather good agreement with a recently obtained measurement of the relaxation time of the PEO 0.1 % through a novel proposed method based on particle migration in a microfluidic channel (Del Giudice et al. 2015). The value of the relaxation time obtained by using this novel method is  $\lambda = 1.74 \times 10^{-3}$  s. In what follows, the value estimated from the Zimm prediction is used in the Deborah number definition. We emphasize, however, that using one or the other estimate for the relaxation time in the definition of the Deborah number does not alter any of the qualitative features emerging from our experiments, except for (slight) quantitative differences.

Figure 1c reports the relative shear viscosity (with respect to the glycerol–water mixture) of the different PEO aqueous solutions as a function of the Deborah number  $De$ . The PEO solution at low concentration (black symbols) shows a constant viscosity behavior in the whole range of Deborah numbers investigated. As the concentration is increased to 0.8 wt% (red symbols), a weak shear thinning appears for  $De \sim 0.3$ . Finally, for the most concentrated PEO solution (gray symbols), a remarkable viscosity-thinning is observed beyond  $De \sim 0.1$  with the viscosity reducing by one order of magnitude over two decades of Deborah numbers.

Polystyrene (PS) particles (Polysciences) with diameter  $D_p = 10$   $\mu$ m and density  $\rho_p = 1.05$  g/ml are used. A dilute suspension with a volume fraction  $\phi = 0.01\%$  is prepared. Particles are added to the matrix that is put first in a mixer (Vortex, Falc Instruments) to guarantee a good dispersion and then in an ultrasonic bath (Falc Instruments) to remove air bubbles. This procedure is repeated before each experiment.

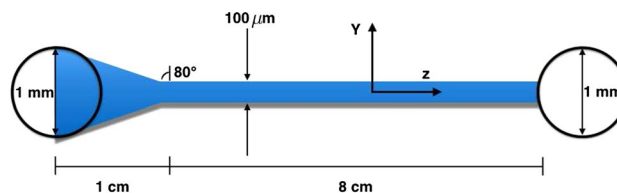


**Fig. 2** Schematic representation of the channel used in the experiments. A smooth entrance at the channel ends is fabricated in order to guarantee an uniform particle distributions. In the figure, the relevant dimensions are reported. The dimensions along  $Y$  and  $Z$  are not in scale

### 3.2 Microfluidic device

Experiments are carried out in a square-shaped cross section channel made of polymethylmethacrylate (PMMA, substrate thickness 1 mm, Goodfellow). The channel is milled on the PMMA substrate using a micromilling machine (Minitech CNC Mini-Mill). A 2-mm tip is first used to mill the whole substrate of 150  $\mu$ m to guarantee level uniformity. A tip with the same dimension of the channel side is, then, inserted in the machine to mill the channel. Finally, two holes are made in the substrate to prepare the access to the inlet and the outlet of the channel (see below). An analysis with a profilometer (Veeco Dektak 150) has been performed to check that the accuracy of the channel depth is within 10 %. Finally, the channel is bonded on another PMMA substrate by immersing the two pieces in absolute ethanol (from Sigma-Aldrich) for about 20 min, clamping them together, and putting the device in the oven at 40  $^{\circ}$ C for about 2 h.

A schematic picture of the channel geometry is reported in Fig. 2. The entrance (triangular shape from the top view, left side of Fig. 2) is designed in such a way to assure a smooth velocity field from the inlet to the main channel (Del Giudice et al. 2013). The relevant dimensions of the device are shown in Fig. 2. The dimension of the cross-sectional side is  $H = 100$   $\mu$ m. Hence, the confinement ratio is  $\beta = D_p/H = 0.1$ .

The flow rate is controlled by a syringe pump (Nemesys) using glass syringes. This machine is able to discriminate different flow rates with a precision of 1 nl/min. The applied flow rates vary in the range  $0.1 \mu\text{l}/\text{min} < Q < 3 \mu\text{l}/\text{min}$ . The achievement of steady-state conditions and the absence of possible leaking are verified through the invariance of the particle velocities.

### 3.3 Particle distributions

Particles flowing in the channel are observed using a straight microscope (Olympus BX-73) with a 4x objective to reach the best field of depth without losing information

on particle motion. Image sequences are collected with a fast camera (IGV-B0620M, Imperx) at a frame rate variable between 30 and 400 fps depending on the flow rate. The observations are all made at a fixed distance of  $L = 8$  cm from channel inlet. The total length of the channel is  $L_{\text{tot}} = 9$  cm. All the experiments are performed at room temperature.

The velocity distributions are measured by particle tracking. To quantify the particle focusing, we evaluate the fraction of particles passing in a certain zone of the square cross section by considering concentric *bands*, as reported in our previous study (Del Giudice et al. 2013). We compute the fraction of particles  $f_k$  in the band  $k$  as (D’Avino et al. 2012; Del Giudice et al. 2013):

$$f_k = \frac{\frac{n_k}{A_k \bar{v}_k}}{\sum_k \frac{n_k}{A_k \bar{v}_k}} \tag{5}$$

where  $n_k$  is the number of particles flowing in the band  $k$  (at  $L = 8$  cm from the inlet),  $A_k$  and  $\bar{v}_k$  are the cross-sectional area and average velocity of the band  $k$ , respectively. The normalization of each  $n_k$  in Eq. (5) through the product  $A_k \bar{v}_k$  in Eq. (5) is made to properly take into account that different bands have different areas and velocities. To obtain a good statistical sample, at each flow rate, we collect a number of frames to get, in total, at least 100 particles.

The procedure adopted to compute the fraction of particles in each band  $f_k$  has been described elsewhere (Del Giudice et al. 2013) and is only briefly reviewed here. The idea is to combine particle tracking visualization and numerical simulations of the fluid velocity profile to locate a particle in a specific position of the channel cross section. Denoting with  $z$  the direction of the flow and with  $x$  and  $y$  the directions parallel to the sides of the cross section, the visualization from the top of the device allows to measure the particle velocity  $V_{p,z}$  as well as the coordinate of the particle center  $x_p$ .

By simulating the velocity profile  $V_{\text{sim},z}(x_p, y_p)$  of the unloaded fluid (see next section), the following equation can be solved:

$$V_{\text{sim},z}(x_p, y_p) = V_{p,z} \tag{6}$$

and the value  $y_p$  is thus computed.

### 3.4 Numerical simulations of the unloaded fluid velocity profile

Numerical simulations of the velocity profile of the fluid without particles in the square-shaped microchannel are performed, to be later used, together with particle tracking experiments, to reconstruct the particle positions. The following governing equations are solved by the finite element method:

$$\nabla \cdot \mathbf{v} = 0 \tag{7}$$

$$-\nabla p + 2\nabla \cdot [\eta(I_D)\mathbf{D}] = \mathbf{0} \tag{8}$$

where  $\mathbf{v}$  is the fluid velocity,  $p$  the pressure,  $\eta(I_D)$  the local shear rate dependent viscosity and  $\mathbf{D} = (\nabla\mathbf{v} + \nabla\mathbf{v}^T)/2$  the rate of deformation tensor. Indeed, the viscosity is a function of the second invariant of the rate of deformation tensor  $I_D \equiv \sqrt{2\mathbf{D} : \mathbf{D}}$  which, in simple shear, becomes  $I_D = \dot{\gamma}$  (Bird et al. 1987). For the constitutive equation  $\eta(\dot{\gamma})$ , we selected the Bird-Carreau model (Bird and Carreau 1968):

$$\eta(\dot{\gamma}) = \eta_\infty + (\eta_0 - \eta_\infty) \frac{1}{[1 + (K I_D)^2]^{\frac{1-n}{2}}} \tag{9}$$

with parameters obtained by fitting the viscosity trends of the experimental fluids reported in Fig. 1c. The curves are superimposed to experimental data. The simulations are performed in a square-shaped microchannel of a  $100 \mu\text{m}$  side, with periodic boundary conditions between inflow and outflow, no slip at the walls and by imposing the experimental flow rates at the inlet section.

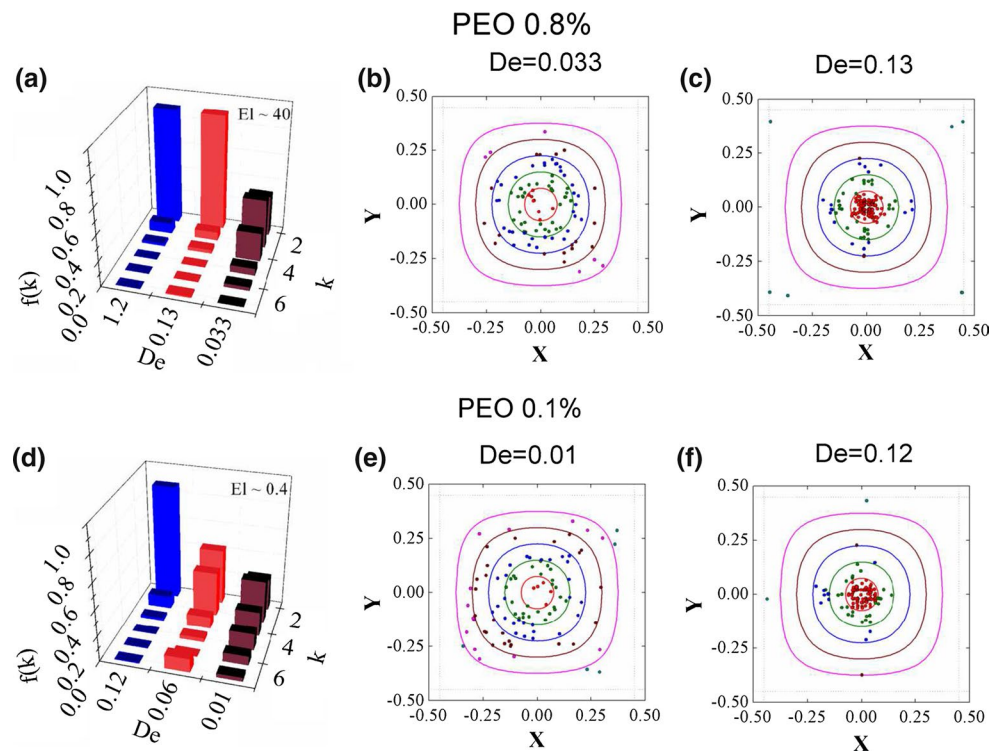
Notice that velocity  $V_{\text{sim},z}$  in Eq. (6) should be the particle velocity, whereas the velocity  $\mathbf{v}$  computed from Eqs. (7)–(9) is the fluid velocity, which is obtained in the absence of the particle. In confined systems, those two velocities are not exactly the same. In particular, in pressure-driven flows, the velocity of the fluid at the same location of the particle center is slightly higher than the particle velocity (it is conventionally stated that the particle *lags* the fluid). For the investigated confinement ratio, the discrepancies between those two velocities are quite small around the channel centerline (Higdon and Muldowney 1995), whereas it might become relevant for particles very close to the walls, i.e., for those particles belonging to the outermost bands. However, we recall that the aim of the procedure adopted to reconstruct the particle positions is that of assigning each particle to a specific band  $k$ . Thus, the most critical situation occurs for those particles lying close to the boundary between the fifth and sixth band for which an overestimation of the velocity will lead to an erroneous assignment of particles to the bands. However, those events are statistically irrelevant in all the cases considered in what follows, and hence, particle distributions are never significantly altered.

## 4 Results

We firstly present the experimental results for the PEO suspending fluid at intermediate concentration (0.8 wt%). As shown in Fig. 1c, the fluid viscosity is essentially constant



**Fig. 3** Experimental results for PEO 0.8 wt% (a–c) and PEO 0.1 wt% (d–f). **a** Fractions of particles in the different band  $k$  measured at 8 cm from the inlet as a function of  $De$ . **b** Particle positions on the square cross section at  $De = 0.033$ . The symbols denote the position of the particle centers and are colored according the band they belong to. **c** Particle positions as in (b), at  $De = 0.13$ . **d** Fractions of particles in the different band  $k$  measured at 8 cm from the inlet as a function of  $De$ . **e** Particle positions as in (b) at  $De = 0.01$ . **f** Particle positions as in (b), at  $De = 0.12$



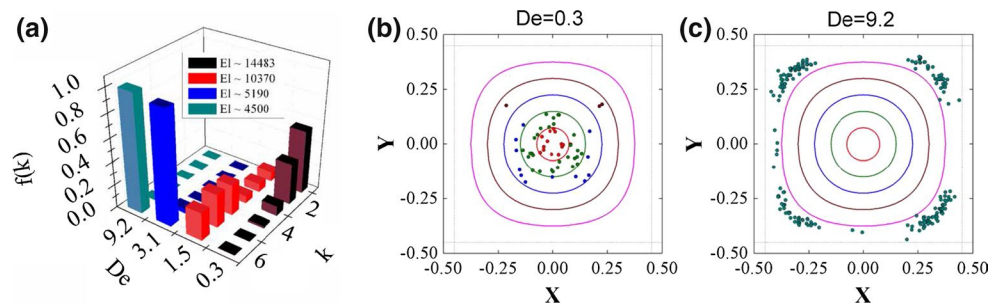
with the Deborah number up to  $De \sim 1$  (corresponding to the maximum flow rate investigated for this fluid), and hence in the range of flow rates investigated for this liquid, the Elasticity number is constant as well. For this set of experiments, we evaluate  $El \sim 40$ , i.e., the fluid elasticity is expected to be dominant with respect to inertia.

Figure 3a reports the fraction of particles in the bands for three different Deborah numbers, whereas Fig. 3b, c shows the reconstruction of the particle positions over the channel cross section for the minimum and maximum values of the Deborah number. It is readily observed that, at  $De = 0.033$ , viscoelastic effects are present but weak: The particles tend to still migrate toward the channel centerline, but at 8 cm from the inlet, they are distributed between the bands  $k = 1$  and  $k = 3$ . By increasing  $De$ , viscoelastic forces become stronger and the most of the particles are more focused in the innermost band. From this first set of experimental results, it clearly appears that particles suspended in a fluid with constant viscosity under elasticity-dominant conditions are subjected to a migration force toward the channel centerline.

Let us now investigate the co-occurring effect of inertia and elasticity on particle migration by selecting the PEO 0.1 wt% as suspending liquid. In this case, indeed, we found that the Elasticity number  $El \sim 0.4$ , which would mean that inertial and viscoelastic forces are comparable. (Notice that, as for the previous case, the fluid viscosity can be assumed constant in the range of flow rates investigated). From the data shown in Fig. 3d, however, we observe a

qualitatively similar situation as the PEO 0.8 wt% case: At low Deborah numbers, the particles are essentially randomly distributed between the bands  $k = 1$  and  $k = 5$  and only the outermost band is empty; as the Deborah number increases, more and more particles move toward the innermost band. For the highest flow rate considered, the most of the particles are confined in the inner two bands and only few of them still belong to the third one. Notice that no particle is anyway found at some equilibrium position between the channel centerline and the walls, or in the corners. It so appears that, even for an Elasticity number around unity, the focusing mechanism induced by the fluid viscoelasticity dominates being essentially unaffected by inertial effects. In other words, even when the Reynolds number becomes comparable with the Deborah number, the effective migration force acting on the particles stays always directed toward the centerline, regardless of the initial particle position, similarly to the purely viscoelastic case.

As a final case, we report in Fig. 4 the migration of particles suspended in the high concentration PEO 1.6 %. Due to the high viscoelasticity of the solution ( $\lambda \sim 0.18$  s), the Deborah number is relatively high even at low flow rates. At the lowest Deborah number here considered ( $De = 0.3$ ), the viscosity is equal to the zero-shear one; at the highest  $De$  number ( $De = 9.2$ ) instead, the viscosity is  $\sim 1.4$  of its zero-shear value (see Fig. 1). In short, except for the lowest  $De$ , the fluid is always in the shear-thinning region of the flow curve for all the examined flow rates. As a



**Fig. 4** Experimental results for PEO 1.6 %. **a** Fractions of particles in the different band  $k$  measured at 8 cm from the inlet as a function of  $De$ . **b** Particle positions on the square cross section at  $De = 0.3$ .

consequence, the Elasticity number will be changing with the flow rate in the experiments. Notice, however, that the smallest Elasticity number is  $El \sim 4500$  (corresponding to  $De = 9.2$ ), i.e., for the PEO 1.6 % suspending fluid, inertial effects are always definitely irrelevant. From Fig. 4a–c, a qualitative difference from the two previous cases is observed. At the lowest Deborah number ( $De = 0.3$ ), particles still migrate toward the centerline in agreement with the previous cases. The presence of the shear thinning, however, does influence the migration phenomenon, because only around 60 % of the particles are focused in the centerline (see Fig. 4b), in contrast with higher percentage values found before. Notice, however, that all the particles are located between the first two bands, somehow confirming the previous results pertaining to lower values of  $\lambda$ . By increasing the Deborah number for the PEO 1.6 %, a different scenario takes place as apparent in Fig. 4: The particles now do not migrate toward the channel centerline, but toward the corners. At  $De = 9.2$ , all the particles belong to the outermost band and are positioned at the corners only, see Fig. 4c. Apparently, also the particles initially located around the channel centerline have been driven outwardly toward the channel corners.

## 5 Discussion

The experimental results presented in the previous section lead us to draw some conclusions about the effect of fluid rheology on the particle migration in viscoelastic fluids, in the square channel geometry.

If the suspending liquid has a constant viscosity, the particles are always found to migrate toward a single equilibrium position represented by the channel centerline. Such a behavior occurs for both the PEO 0.1 and 0.8 % and agrees with previous experiments (Del Giudice et al. 2013) in a PVP suspending liquid (that is an elastic, but constant viscosity fluid) as well with numerical simulations (Villone et al. 2013). In this situation, the flow rate only

The *symbols* denote the position of the particle centers and are *colored* according the band they belong to. **c** Particle positions as in **(b)**, at  $De = 9.2$

quantitatively affects the migration mechanism by enhancing the transversal motion toward the centerline, according to previous theoretical predictions in different channel geometries (Leshansky et al. 2007; D’Avino et al. 2012).

Fluid shear thinning (always combined with elasticity) strongly alters the scenario, as observed for PEO 1.6 %. At low Deborah numbers, i.e., in the fluid constant viscosity region, particles migrate toward the centerline, as in the previous cases of PEO 0.1 % and PEO 0.8 %. At very high Deborah numbers, conversely, i.e., in the fluid shear-thinning region, the migration direction is reversed and particles are driven toward the channel corners. Except for a previous single observation in a cylindrical channel (D’Avino et al. 2012), to the best of our knowledge, this is the first experimental measurement of the effect of the fluid shear thinning on particle migration.

The motion toward the channel corners reported in the present paper, occurring at high  $De$  for shear-thinning fluids, agrees with recent 3D finite element simulations where the motion of a single spherical particle suspended in liquids modeled through several constitutive equations and flowing in a square-shaped microchannel under inertialess conditions is investigated (Villone et al. 2013). In that work, for fluids with a zero second normal stress difference (for which secondary flows are absent), the numerical predictions show that the particle migrates toward the channel centerline or the corners depending on its initial position. The two migration directions are separated by a closed curve. The position of such a curve strongly depends on the constitutive and flow parameters and, in particular, on the entity of the shear thinning. For strongly shear-thinning fluids and high  $De$ , the separatrix approaches the channel centerline and wall attraction results.

Let us quantify the just described transition. At low Deborah numbers, where the constitutive equation considered in the simulations in Villone et al. (2013) is well approximate by an Oldroyd-B model, with constant viscosity, the separatrix is calculated to be quite close to the channel walls, implying that almost all the particles focus toward

the channel centerline. Specifically, the area of the cross section pertaining to centerline attractor is 85 % of the entire cross section, as readily estimated from Fig. 4 of Villone et al. (2013). This estimate is in qualitative agreement with our experimental results on PEO 0.1 %, PEO 0.8 % and PEO 1.6 % at low Deborah numbers, in the sense that we always observed focusing toward the centerline in those cases. The simulation results in Villone et al. (2013) further show that, at  $De = 6$ , the separatrix has become quite close to the centerline: The area of the cross section pertaining to centerline attractor has decreased to 5% of the entire cross section. Most of the particles are then predicted to be driven outwardly toward the walls, fully consistently with our experiments.

For the sake of precision, it should be remarked that the simulations always predict the existence of a region (although narrow for high  $De$ -values) around the channel centerline such that the particles migrate inwardly toward the cross-section center. On the other hand, in our experiments, we do not find a coexistence of corner- and center-attractive equilibrium positions. Such a discrepancy might perhaps be ascribed to the constitutive parameters chosen in the simulations, which do not exactly describe the rheology of PEO 1.6 %. In particular, the simulations in Villone et al. (2013) are performed for a single-relaxation time fluid, whereas the measured dynamic response of PEO 1.6 % reported in Fig. 1b suggests that a multi-mode constitutive equation would be more appropriate.

The second important conclusion obtained here is the negligible effect of inertia with respect to elasticity on the focusing mechanism. By varying the Elasticity number over almost two order of magnitude (from  $El \sim 0.4$  to  $El \sim 40$ ), no qualitative change in the final particle position (the centerline) is observed, suggesting that the migration induced by viscoelasticity is, as a matter of fact, the only relevant mechanism for elastic, constant viscosity fluids. In this regard, we mention recent experiments (Choi et al. 2011) on particle migration induced by inertial effects in Newtonian fluids flowing in square-shaped microchannel. They have found that particles confined in a channel with  $\beta \sim 0.1$  experience a very limited migration across the streamline within 10 cm of channel length even at  $Re \sim 7$ . Only by increasing the Reynolds number up to  $Re \sim 50$ , a transversal motion toward four attractors located at the center of each face is found. A similar situation has also been reported in a cylindrical channel (Seo et al. 2014). In other words, for a fixed confinement ratio  $\beta$ , the condition  $\mathcal{O}(De) = \mathcal{O}(Re)$ , corresponding to  $\mathcal{O}(El) = 1$ , seems to denote a situation where the particle migration is distinctly governed by elastic effects rather than inertial ones.

An idea about the relative strength of elasticity and inertia on particle migration can be given by comparing the theoretical expressions for the migration velocity due to

elastic and inertial effects. In Poiseuille tube flow, the inertial migration velocity can be expressed as (Ishii and Hasimoto 1980):

$$\left|V_m^{\text{in}}\right| = B Re_c \beta^3 \frac{r}{R} \quad (10)$$

where  $r$  and  $R$  are the particle radial position and the tube radius, respectively,  $B$  is a constant and  $Re_c = \rho \bar{U}R/\eta$  the Reynolds number defined for a cylindrical channel with average velocity  $\bar{U}$ .

In the same flow field, the migration velocity due to elasticity is (D'Avino et al. 2012):

$$\left|V_m^{\text{el}}\right| = A De_c \beta^2 \frac{r}{R} \quad (11)$$

with  $A$  a constant and  $De_c = \lambda \bar{U}/(2R)$  the Deborah number defined for a cylindrical channel. Both relationships hold around the channel centerline and for small confinement ratios and flow rates. From the two expressions above, we get:

$$\left|\frac{V_m^{\text{in}}}{V_m^{\text{el}}}\right| = \frac{B Re_c}{A De_c} \beta = \frac{B}{A} \frac{1}{El} \beta \quad (12)$$

By taking the values of the constants  $A \approx 6.6$  and  $B \approx 1.4$  from D'Avino et al. (2012) and Ishii and Hasimoto (1980), respectively, an estimate of the right-hand side for the less concentrated PEO solution used in this work (corresponding to the smallest Elasticity number available in our experiments,  $El \sim 0.4$ ) gives that the ratio of the migration velocities is about  $5 \times 10^{-2}$ , confirming that inertial effects are much smaller than the elastic ones. Therefore, from Eq. (12) appears that the Elasticity number alone gives misleading indications about the relative strength of inertia and viscoelasticity, and one should account for the confinement ratio as well as the correct prefactor  $B/A$ . A similar conclusion concerning the inability of the Elasticity number alone to describe the relative effects of inertia and viscoelasticity can be reached by looking at the results reported in Lim et al. (2014). In that work, indeed, the authors succeeded in going down to  $El = 0.05$ , and nevertheless found focusing toward the centerline, as in a purely viscoelastic situation. We would also like to signal that recent 2D simulations of the coupled inertia–viscoelastic case (Trofa et al. 2014) appear to confirm that  $Re$  much larger than  $De$  is needed (by at least one order of magnitude) to appreciate deviations from the purely viscoelastic case.

Whether or not the conclusions derived from Eq. (12) also apply for confinement ratios or flow rates higher than those considered in this work cannot be assessed yet. Further experiments and numerical simulations accounting for the simultaneous effects of elasticity and inertia would be helpful in this direction.



## 6 Conclusions

In this work, we have studied the effect of fluid rheology on particle migration in a square-shaped microchannel. To this aim, we have prepared and rheologically characterized three PEO solutions at different concentrations with increasing level of elasticity and shear thinning. Experiments at different flow rates are carried out. Measurements are taken at a fixed distance from the inlet  $L = 8$  cm, and the particle positions over the channel cross section are recovered by combining a particle tracking method with 3D numerical simulations (Del Giudice et al. 2013).

Our results show that particles suspended in a constant viscosity fluid are focused toward the channel centerline due to the medium elasticity. Such an inward migration occurs even at the lowest Elasticity number ( $El \sim 0.4$ ) for which one could expect that inertial effects (working in opposite direction as the viscoelastic ones) play a role. Since our experiments do not show any qualitative change from the high Elasticity number case, we conclude that elastic forces are much stronger than the inertial ones when the two representative dimensionless numbers ( $De$  and  $Re$ ) are of the same order of magnitude and hence  $El \sim 1$ . Indeed, the relevant dimensionless parameter should account for the confinement ratio as well as a prefactor ‘measuring’ the relative strength of the inertial and viscoelastic migration velocities. Finally, strongly shear-thinning fluids qualitatively alter the scenario; in particular, particles migrate toward the channel centerline when exploring the fluid constant viscosity region, whereas at high flow rate, i.e., in the fluid shear-thinning region, particles are pushed toward the corners of the channel cross section.

## References

- Bhagat AAS, Kuntaegowdanahalli SS, Kaval N, Seliskar CJ, Papautsky I (2010) Inertial microfluidics for sheath-less high-throughput flow cytometry. *Biomed Microdevices* 12(2):187–195
- Bird RB, Carreau PJ (1968) A nonlinear viscoelastic model for polymer solutions and melts I. *Chem Eng Sci* 23(5):427–434
- Bird RB, Armstrong RC, Hassager O (1987) *Dynamics of polymeric liquids: fluid mechanics*. Wiley-Interscience, New York
- Cavallaro M, Botto L, Lewandowski EP, Wang M, Stebe KJ (2011) Curvature-driven capillary migration and assembly of rod-like particles. *Proc Natl Acad Sci* 108(52):20923–20928
- Choi YS, Seo KW, Lee SJ (2011) Lateral and cross-lateral focusing of spherical particles in a square microchannel. *Lab Chip* 11(3):460–465
- D’Avino G, Romeo G, Villone MM, Greco F, Netti PA, Maffettone PL (2012) Single line particle focusing induced by viscoelasticity of the suspending liquid: theory, experiments and simulations to design a micropipe flow-focuser. *Lab Chip* 12(9):1638–1645
- Del Giudice F, Romeo G, D’Avino G, Greco F, Netti PA, Maffettone PL (2013) Particle alignment in a viscoelastic liquid flowing in a square-shaped microchannel. *Lab Chip* 13(21):4263–4271
- Del Giudice F, D’Avino G, Greco F, De Santo I, Netti PA, Maffettone PL (2015) Rheometry-on-a-chip: measuring the relaxation time of a viscoelastic liquid through particle migration in microchannel flows. *Lab Chip* 15:783–792
- Di Carlo D (2009) Inertial microfluidics. *Lab Chip* 9(21):3038–3046
- Gijs MA (2004) Magnetic bead handling on-chip: new opportunities for analytical applications. *Microfluid Nanofluid* 1(1):22–40
- Graessley WW (1982) In: *Synthesis and degradation rheology and extrusion* Springer, pp 67–117
- Higdon J, Muldowney G (1995) Resistance functions for spherical particles, droplets and bubbles in cylindrical tubes. *J Fluid Mech* 298:193–210
- Ho B, Leal L (1974) Inertial migration of rigid spheres in two-dimensional unidirectional flows. *J Fluid Mech* 65(02):365–400
- Ishii K, Hasimoto H (1980) Lateral migration of a spherical particle in flows in a circular tube. *J Phys Soc Jpn* 48:2144–2155
- Kang K, Lee SS, Hyun K, Lee SJ, Kim JM (2013) DNA-based highly tunable particle focuser. *Nat Comm* 4:2567
- Lee DJ, Brenner H, Youn JR, Song YS (2013) Multiplex particle focusing via hydrodynamic force in viscoelastic fluids. *Sci Rep* 3:3258
- Leshansky A, Bransky A, Korin N, Dinnar U (2007) Tunable nonlinear viscoelastic ‘focusing’ in a microfluidic device. *Phys Rev Lett* 98(23):234501
- Liang L, Ai Y, Zhu J, Qian S, Xuan X (2010) Wall-induced lateral migration in particle electrophoresis through a rectangular microchannel. *J Colloid Interface Sci* 347(1):142–146
- Lim EJ, Ober TJ, Edd JF, Desai SP, Neal D, Bong KW, Doyle PS, McKinley GH, Toner M (2014) Inertio-elastic focusing of bioparticles in microchannels at high throughput. *Nat Comm* 5:4520
- Lim H, Nam J, Shin S (2014) Lateral migration of particles suspended in viscoelastic fluids in a microchannel flow. *Microfluid Nanofluid*, pp 1–10
- Martel JM, Toner M (2013) Particle focusing in curved microfluidic channels. *Sci Rep* 3:1–8
- Nam J, Lim H, Kim D, Jung H, Shin S (2012) Continuous separation of microparticles in a microfluidic channel via the elasto-inertial effect of non-Newtonian fluid. *Lab Chip* 12(7):1347–1354
- Pamme N (2006) Magnetism and microfluidics. *Lab Chip* 6(1):24–38
- Pamme N (2007) Continuous flow separations in microfluidic devices. *Lab Chip* 7(12):1644–1659
- Rodd LE, Scott TP, Boger DV, Cooper-White JJ, McKinley GH (2005) The inertioelastic planar entry flow of low-viscosity elastic fluids in micro-fabricated geometries. *J Non-Newtonian Fluid* 129(1):1–22
- Rodd L, Cooper-White J, Boger D, McKinley G (2007) Role of the elasticity number in the entry flow of dilute polymer solutions in micro-fabricated contraction geometries. *J Non-Newtonian Fluid* 143(2):170–191
- Romeo G, D’Avino G, Greco F, Netti PA, Maffettone PL (2013) Viscoelastic flowfocusing in microchannels: scaling properties of the particle radial distributions. *Lab Chip* 13(14):2802–2807
- Segré G, Silberberg A (1961) Radial particle displacements in Poiseuille flow of suspensions. *Nature* 189:209–210
- Seo KW, Byeon HJ, Huh HK, Lee SJ (2014) Particle migration and single-line particle focusing in microscale pipe flow of viscoelastic fluids. *RSC Adv* 4(7):3512–3520
- Shields CW, Johnson LM, Gao L, López GP (2014) Elastomeric negative acoustic contrast particles for capture. Acoustophoretic transport and confinement of cells in microfluidic systems. *Langmuir* 30(14):3923–3927
- Skowronek V, Rambach RW, Schmid L, Haase K, Franke T (2013) Particle deflection in a poly (dimethylsiloxane) microchannel using a propagating surface acoustic wave: size and frequency dependence. *Anal Chem* 85(20):9955–9959

- Tirtaatmadja V, McKinley GH, Cooper-White JJ (2006) Drop formation and breakup of low viscosity elastic fluids: effects of molecular weight and concentration. *Phys Fluids* 18(4):043101
- Trofa M, Vocciante M, D'Avino G, Hulsén MA, Greco F, Maffettone PL (2014) Numerical simulations of the competition between the effects of inertia and viscoelasticity on particle migration in Poiseuille flow. *Comput Fluids* 107:214–223
- van der Zande BM, Koper GJ, Lekkerkerker HN (1999) Alignment of rod-shaped gold particles by electric fields. *J Phys Chem B* 103(28):5754–5760
- Villone M, D'Avino G, Hulsén M, Greco F, Maffettone P (2013) Particle motion in square channel flow of a viscoelastic liquid: migration vs. secondary flows. *J Non-Newtonian Fluid* 195:1–8
- Whitesides GM (2006) The origins and the future of microfluidics. *Nature* 442(7101):368–373
- Xuan X, Zhu J, Church C (2010) Particle focusing in microfluidic devices. *Microfluid Nanofluid* 9(1):1–16
- Yamaguchi K, Matsumoto K, Fujii T (1990) Magnetic anisotropy by ferromagnetic particles alignment in a magnetic field. *J Appl Phys* 67(9):4493–4495
- Yang S, Kim JY, Lee SJ, Lee SS, Kim JM (2011) Sheathless elastoinertial particle focusing and continuous separation in a straight rectangular microchannel. *Lab Chip* 11(2):266–273
- Yang S, Lee SS, Ahn SW, Kang K, Shim W, Lee G, Hyun K, Kim JM (2012) Deformability-selective particle entrainment and separation in a rectangular microchannel using medium viscoelasticity. *Soft Matter* 8(18):5011–5019
- Yeo LY, Friend JR (2014) Surface acoustic wave microfluidics. *Annu Rev Fluid Mech* 46:379–406
- Zeng J, Deng Y, Vedantam P, Tzeng TR, Xuan X (2013) Magnetic separation of particles and cells in ferrofluid flow through a straight microchannel using two offset magnets. *J Magn Mater* 346:118–123
- Zhou J, Papautsky I (2013) Fundamentals of inertial focusing in microchannels. *Lab Chip* 13(6):1121–1132